Eu^{2+}-sensitized Mn^{2+} luminescence in $RbMgF_3$:Eu,Mn

M. D. Shinn and W. A. Sibley
Physics Department, Oklahoma State University, Stillwater, Oklahoma 74078
(Received 1 August 1983)

Energy transfer from Eu^{2+} to Mn^{2+} ions is shown to occur in $RbMgF_3$:Eu,Mn crystals. Emission and excitation spectra indicate that the energy transfer is a resonant process between the Eu^{2+} $^6P_{7/2}\rightarrow{}^8S_{7/2}$ emission and the Mn^{2+} $^6A_{1g}\rightarrow{}^4T_{2g}^2$ absorption levels. The energy transfer is so efficient, even at low dopant concentrations of $\sim$2000 ppm, that at these low concentrations energy transfer must occur between copious Eu^{2+}-Mn^{2+} close pairs. These Eu^{2+}-Mn^{2+} pairs form preferentially in the lattice. For higher Mn^{2+} concentrations the energy transfer occurs not only among Eu^{2+}-Mn^{2+} pairs, but also between Eu^{2+} and Mn^{2+} ions.

I. INTRODUCTION

Sensitized luminescence was first theoretically treated for systems with allowed (electric dipole) transitions by Förster,[1-3] and was extended for other multipolar transitions by Dexter.[4] Further development of the effects of exchange coupling was made by Inokuti and Hirayama.[5] The migration of energy among the initially excited ions (sensitizers) before transfer to the other set of ions (activators) was studied by Yokota and Tanimoto.[6]

In the simplest case, impurity-sensitized luminescence is a single-step process which occurs when the emission of the sensitizer is in resonance with the absorption of the activator. The rate of transfer can then be found using time-dependent perturbation theory. The time dependence of the sensitizer luminescence decay depends on the form of multipole coupling. Experimental determination of the type of coupling and the energy transfer rate may be made by measurements of the sensitizer luminescence following pulse excitation. There are numerous examples in the literature of the usefulness of this approach.[1-10]

We have previously conducted a number of investigations on the optical properties of both radiation-induced centers and impurities in $RbMgF_3$ crystals.[11-19] Samples doped with low ($\leq$20 at. %) concentrations of Mn^{2+} normally exhibit only a weak orange emission.[13] Following the observation of energy transfer between Er^{3+} and Mn^{2+} ions in this material,[16,17] samples of $RbMgF_3$:Eu,Mn were grown to help clarify the nature of this interaction. These crystals were found to produce intense Mn^{2+} emission under ultraviolet excitation, which is suggestive of sensitized luminescence.

In this paper the process of the impurity-sensitized luminescence of Mn^{2+} in $RbMgF_3$:Eu,Mn is investigated. It is shown that the efficient energy transfer is due to the presence of copious Eu^{2+}-Mn^{2+} ion pairs in this crystal. This is in contrast to most impurity-sensitized luminescence situations, where a uniform distribution of sensitizers and activators throughout the host material occurs.

II. EXPERIMENTAL METHODS

The crystals used in this study were grown by C. A. Hunt of the Oklahoma State University Crystal Growth Facility in an inert atmosphere using the Bridgeman technique. Two crystals were grown, one with initial melt concentrations $RbMg_{0.98}Mn_{0.01}F_3$:$Eu_{0.01}$, the other with initial melt concentrations $RbMg_{0.84}Mn_{0.15}F_3$:$Eu_{0.01}$. The impurities were added in the form of MnF_2 and $EuCl_3$. Some NH_4HF_2 was also added to the starting material to fluorinate the $EuCl_3$, and to act as an oxygen getter. The resulting crystals were of good optical quality.

For low-temperature measurements, a Sulfrian helium cryostat, or a CTI Cryogenics Cryodyne Cryocooler Model 21SC were utilized. High-temperature measurements were made with the sample enclosed in a copper holder with small windows for the excitation and emission light. Temperature control was accomplished using resistance heaters. Temperature control below room temperature was within $\pm$1 K, while above room temperature it was $\pm$5 K.

Emission and excitation spectra measurements were made by exciting the samples with light from a 75-W xenon-arc lamp passed through a 0.22-m Spex monochromator. The excitation spectra were corrected for variations in the lamp intensity and monochromator response using the flat response of a 0.05 mg/ml solution of rhodamine *B* in ethylene glycol. The fluorescence was focused into a 0.8-m Spex monochromator and mirrors sent the emerging light to a cooled RCA C31034 photomultiplier tube (PMT). The monochromator and detector response was corrected using a quartz-iodine lamp traceable to the National Bureau of Standards. The signal from the PMT was preamplified and passed to a lock-in amplifier that was synchronized with a variable-speed light chopper in the excitation beam. The output of the lock-in amplifier may be displayed on an *X-Y* recorder or stored by a Hewlett-Packard HP-85 minicomputer. Lifetime measurements longer than 10 μs were made utilizing a Biomation 610B transient recorder and a Nicholet 1070 signal averager. The excitation was either the chopped excitation beam or the filtered light from a General Radio 1538A Strobotac xenon flashlamp. Lifetimes shorter than 10 μs were measured using a Molectron uv 14 nitrogen laser (λ_{ex}=337.1 nm) and a Princeton Applied Research 162 boxcar integrator in the laboratory of R. C. Powell. Optical-absorption measurements were made using a Cary

14 spectrophotometer with 0—0.1 and 0—1.0 OD (optical density) slidewires or a Perkin-Elmer 330 spectrophotometer.

III. EXPERIMENTAL RESULTS

The normalized room-temperature absorption spectra of samples of $RbMgF_3$:Eu and $RbMgF_3$:Eu,Mn are shown in Fig. 1. The broad, intense absorption with maxima near 250 nm is due to transitions from the $4f^7$ ground-state configuration ($^8S_{7/2}$) to the $4f^65d^1$ excited-state configurations[18] and is characteristic of all samples. The maximum absorption coefficient of this band varied from sample to sample and was in the range 150—300 cm^{-1}. This corresponds to an estimated Eu^{2+} concentration of 0.15—0.30 at.%.[20] The weak absorption line at 31 955 cm^{-1} (312.9 nm) present in all samples, including those with no Mn^{2+} has not been reported previously. This may be one of the transitions $4f^7(^8S_{7/2})\rightarrow 4f^6(^7F_J)5d^1$ ($J=0$—6) which has often been reported earlier for other types of Eu^{2+}-doped crystals, and gives the lower energy band a characteristic "staircase" structure.[21] Weak bands due to absorption from the Mn^{2+} $^6A_{1g}$ ground state to excited states up to the $^4T_{2g}^2$ level (the Mn^{2+} ion resides in sites of C_{3v} symmetry, but for simplicity O_h symmetry assignments of the Mn^{2+} levels will be used) were also detected in the absorption spectrum of the $RbMg_{0.84}Mn_{0.15}F_3$:$Eu_{0.01}$ samples.

The assignments of these bands have been made previously.[13] The oscillator strength of the $^4T_{1g}$ band at $\sim$19 048 cm^{-1} (525 nm) is almost constant in similar hosts.[22,23] With the use of the appropriate form of Smakula's equation[24]

$$fN=7.23\times10^{15}\alpha_m W \quad (1)$$

with $\alpha_m=0.1$ cm^{-1}, $W=0.186$ eV, and $f=3.5\times10^{-7}$, the Mn^{2+} concentration was determined to be 3.8×10^{20} cm^{-3} (3.1 at.%). This crystal will be designated the $Mn_{0.03}{}^{2+}$ specimen. The Mn^{2+} concentration of the $RbMg_{0.98}Mn_{0.01}F_3$:$Eu_{0.01}$ samples was too low to be determined from absorption measurements. Instead, the ratio of the excitation peak intensity of the $^4T_{1g}$ band for the $RbMg_{0.98}Mn_{0.01}F_3$:$Eu_{0.01}$ and $Mn_{0.03}{}^{2+}$ samples, was used to determine that the $RbMg_{0.98}Mn_{0.01}F_3$:$Eu_{0.01}$ specimen contained approximately 2.8×10^{19} cm^{-3} (0.2 at.%) Mn^{2+}. This value is consistent with previous mass spectrographic analyses of $RbMgF_3$:Mn crystals with the same starting material concentration of Mn^{2+}. It is also consistent with the concentration found from statistically produced F-center—Mn^{2+} pairs which implies that the Mn^{2+} ions are randomly distributed in the samples.[11,17,25] This crystal will be referred to as the $Mn_{0.002}{}^{2+}$ crystal.

The emission spectra of the $Mn_{0.002}{}^{2+}$ and $Mn_{0.03}{}^{2+}$ samples at room temperature are portrayed in Figs. 2(a) and 2(b). The line emission at $\sim$27 778 cm^{-1} (360 nm) and the band emission at $\sim$24 691 cm^{-1} (405 nm) are due to Eu^{2+} f-f and d-f transitions, respectively. The previously reported band emission at $\sim$19 048 cm^{-1} (525 nm) (Ref. 18) is also present for excitation wavelengths between 330 and 400 nm. The broad emission band around 600 nm arises from the Mn^{2+} transition $^4T_{1g}\rightarrow{}^6A_{1g}$. The Mn^{2+} emission band peaks at 17 094 and 16 450 cm^{-1} for the $Mn_{0.002}{}^{2+}$ and $Mn_{0.03}{}^{2+}$ crystals, respectively. The emission is present from 7 to 500 K, but the peak position and width are temperature dependent, as is also shown in Fig. 2. The room-temperature, high-resolution emission spectra of the Eu^{2+} f-f transitions for the two types of samples are similar to those reported earlier.[18] There are lines around 28 289 cm^{-1} (353.5 nm) which are present in all samples. The intensity of these lines is much weaker than the intensity of the $\sim$359-nm line emissions, and decreases as the temperature decreases. The peak energy and behavior of these emissions are consistent with the previously observed[26,27] Eu^{2+} transitions $^6P_{5/2}\rightarrow{}^8S_{7/2}$, which have been thermalized from the $^6P_{7/2}$ level.

The low-temperature, high-resolution emission spectra for the f-f transitions of $RbMgF_3$:Eu and the $Mn_{0.002}{}^{2+}$ and $Mn_{0.03}{}^{2+}$ samples are presented in Figs. 3(a), 3(b), and

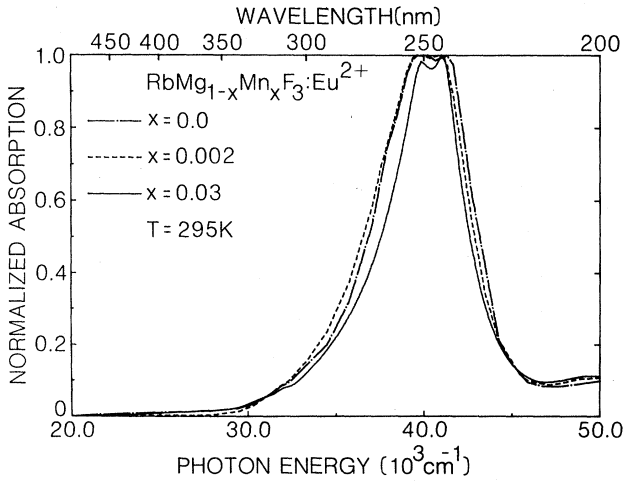

FIG. 1. Normalized absorption spectrum of $RbMgF_3$:Eu^{2+}:$Mn_{0.03}{}^{2+}$ (solid line), $RbMgF_3$:Eu^{2+}:$Mn_{0.002}{}^{2+}$ (dashed line), and $RbMgF_3$:Eu^{2+} (dotted-dashed line) at 295 K.

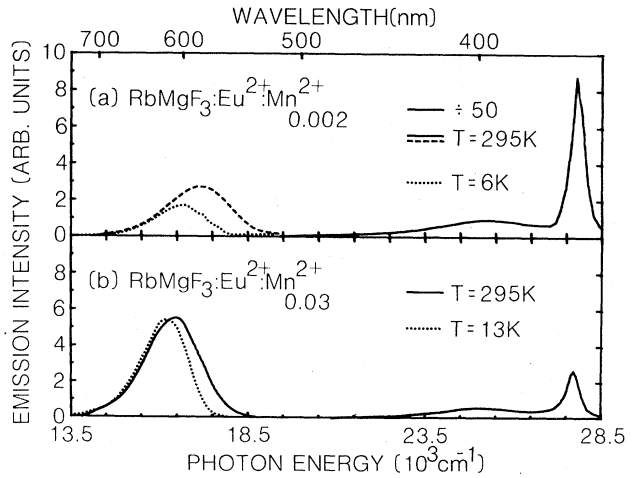

FIG. 2. (a) Emission spectrum of $RbMgF_3$:Eu^{2+}:$Mn_{0.002}{}^{2+}$ at 295 K. Bands plotted as solid lines have had their intensities reduced a factor of 50. Also plotted is the Mn^{2+} emission at 6 K. (b) Emission spectrum of $RbMgF_3$:Eu^{2+}:$Mn_{0.03}{}^{2+}$ at 295 K (solid line). Also plotted is the Mn^{2+} emission at 13 K. In both figures the resolution was 6 nm and $\lambda_{ex}=320$ nm.

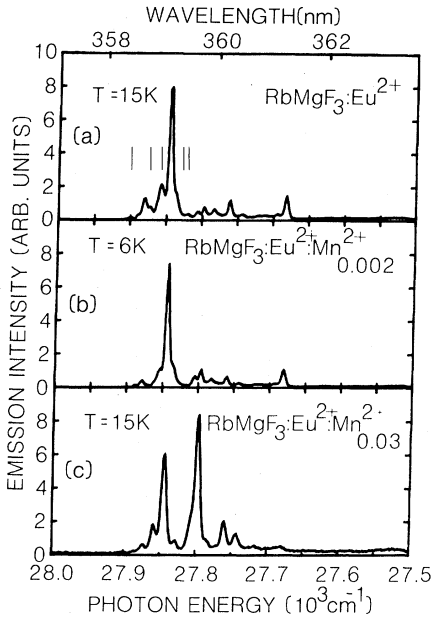

FIG. 3. Low-temperature Eu^{2+} emission spectrum of (a) $RbMgF_3:Eu^{2+}$, (b) $RbMgF_3:Eu^{2+}:Mn_{0.002}{}^{2+}$, and (c) $RbMgF_3:Eu^{2+}:Mn_{0.03}{}^{2+}$. The vertical lines in (a) indicate the position of lines which appear as the temperature is increased. In all figures the resolution was 0.25 Å and $\lambda_{ex}=318$ nm.

3(c), respectively. The similarity between the spectra of $RbMgF_3$:Eu and the $Mn_{0.002}{}^{2+}$ sample should be noted. In contrast the $Mn_{0.03}{}^{2+}$ sample's spectrum shows a weaker line at 27 682 cm^{-1} (361.25 mm) and a stronger line at 27 793 cm^{-1} (359.8 nm). As was previously noted,[18] the relative intensities of these lines change slightly for different samples from each boule, although the line at 27 847 cm^{-1} (359.1 nm) is always one of the most intense lines.

Because of the small splitting (<0.2 cm^{-1}) of the ground state[18,28,29] each ${}^6P_{7/2}\rightarrow{}^8S_{7/2}$ transition of an Eu^{2+} ion in a noncubic site can give rise to no more than four emission lines.[26,30] At 15 K ($kT\approx10$ cm^{-1}) appreciable thermalization of all four levels is not likely. Nevertheless, inspection of Figs. 3(a) and 3(b) reveals at least 12 lines. The temperature dependence of the lines can help determine how many of these lines arise from ions in different sites. As the temperature is increased, five emission lines, whose positions are indicated in Fig. 3(a) by vertical lines, increase in intensity. The change in intensity of these lines at 15, 20, 30, and 40 K was fitted by the simple Boltzmann equation

$$n=n_0\exp(-\Delta E/kT)\ . \tag{2}$$

This analysis suggests that the three highest energy lines are due to thermalization of the 27 847-cm^{-1} (359.1-nm) line. This analysis yields multiplet splittings of 14, 28, and 59 cm^{-1}. The other two lines, at 27 828 (359.36 nm) and 27 813 are due to thermalization of the levels at 27 781 cm^{-1} (359.96 nm) and 27 759 cm^{-1} (360.25 nm), respectively. The splittings are 47 and 54 cm^{-1}. The lower-lying sublevels in these multiplets are obscured by the other transitions. These other emissions decrease at varying rates as the temperature is raised and the 361.25-nm emission is totally quenched by 40 K.

Since the excitation spectra of all emissions from a given submultiplet will be identical, the spectra of the more resolved lines in Fig. 3 were measured. The spectra for these lines all differed and in general tended to shift to lower energy as the emission energy decreases. This was particularly noticeable for the transitions at 360.5 and 361.25 nm.

The luminescence decays of the lines portrayed in Fig. 3 are listed in Table I. At this temperature most of the decay curves were not single exponential. The values listed are the first e^{-1} times. The error in these measurements is $\sim10\%$. The deviation from single-exponential behavior becomes larger as the energy of the transition decreases. There is also a trend toward shorter decay times as the transition energy decreases.

The temperature dependence of the 359.1-nm transition lifetimes for all three crystals is depicted in Fig. 4. The lifetime of the Eu^{2+} band emission at 405 nm was measured at 78 K. The lifetime of this transition in the $Mn_{0.002}{}^{2+}$ samples was found to be approximately 1.6 μs, comparable to the room-temperature value. The e^{-1} time of the band in the $Mn_{0.03}{}^{2+}$ samples was found to be approximately 0.75 μs. The decay was highly nonexponential with a third e-folding time of 1.3 μs.

The 295-K excitation spectra of the Mn^{2+} emission at 600 nm for both Mn^{2+}-doped samples are illustrated in Figs. 5(a) and 5(b), respectively. The highest energy band is due to the Eu^{2+} f-d transition, while the lower energy bands arise from Mn^{2+} ion transitions.[13]

TABLE I. Lifetimes of Eu^{2+} transitions in $RbMgF_3$ and $RbMgF_3$:Mn at 14 K.

Wavelength (nm)	Energy (cm^{-1})	Lifetimes (ms) $RbMgF_3$:Eu	$RbMgF_3$:Eu,Mn ($Mn_{0.002}{}^{2+}$ samples)	$RbMgF_3$:Eu,Mn ($Mn_{0.03}{}^{2+}$ samples)
358.4	27 902		3.10	
358.9	27 863	2.41	2.44	
359.1	27 847	1.84	1.88	1.23
359.8	27 793	2.18	1.84	1.43
360.25	27 759	1.18	1.16	1.05
360.5	27 739	0.048	0.050	
360.9	27 709		1.02	
361.25	27 682	0.123	0.075	

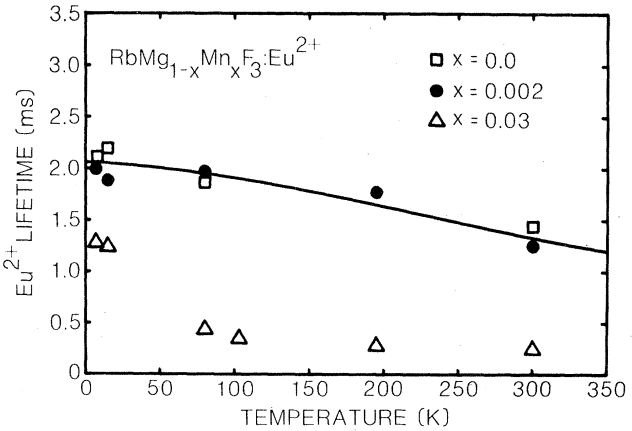

FIG. 4. Temperature dependence of the 359.1-nm Eu^{2+} emission lifetime in $RbMgF_3:Eu^{2+}$ (□), $RbMgF_3:Eu^{2+}:Mn_{0.002}{}^{2+}$ (●), and $RbMgF_3:Eu^{2+}:Mn_{0.03}{}^{2+}$ (△). $\lambda_{ex}=318$ nm.

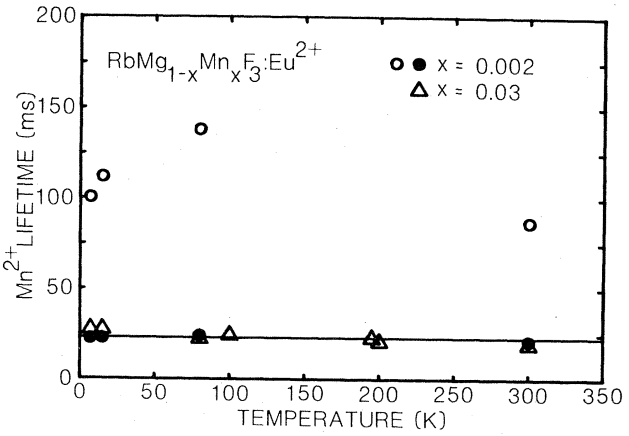

FIG. 6. Temperature dependence of the Mn^{2+} emission lifetime in $RbMgF_3:Eu^{2+}:Mn_{0.002}{}^{2+}$ (○,●) and $RbMgF_3:Eu^{2+}:Mn_{0.03}{}^{2+}$ (△). $\lambda_{ex}=540$ nm.

The response of the Mn^{2+} luminescence after excitation differs for the $Mn_{0.002}{}^{2+}$ and $Mn_{0.03}{}^{2+}$ samples. The temperature dependence of the decay times is shown in Fig. 6. The Mn^{2+} luminescence decay of the $Mn_{0.03}{}^{2+}$ samples after excitation of the $^4T_{1g}$ level (525 nm) exhibited single-exponential decay. Pulsed excitation of the Eu^{2+} band resulted in a large initial luminescence followed by a rise in intensity with the maximum intensity occurring at a time $t_{max}=780$ μs. This value of t_{max} was temperature independent from 14 to 300 K. The decay of the luminescence was nonexponential and had the same e^{-1} time as was measured exciting the Mn^{2+} ion directly. The decay became more single exponential in behavior as the temperature was raised and was single exponential above 200 K.

The decay of the Mn^{2+} luminescence in the $Mn_{0.002}{}^{2+}$ samples after excitation of the $^4T_{1g}$ level was the sum of *two* exponentials. The faster decay, denoted by closed circles, had a temperature-independent lifetime of ~25 ms. The slower decay, denoted by open circles, had a lifetime of ~120 ms for temperatures below 200 K and decreased to 87 ms at 300 K. Pulse excitation of the Eu^{2+} band showed no measurable rise time of the Mn^{2+} luminescence. The luminescence decayed in the same way as for direct excitation of the Mn^{2+} ions.

An interesting new effect was found for the $Mn_{0.002}{}^{2+}$ samples. After chopper excitation of the Eu^{2+} band, the decay was the same as reported for the directly excited Mn^{2+} ions. However, the contribution of the longer lifetime decay to the total intensity of the decay was much larger for the Mn^{2+} ions following Eu^{2+} excitation than for the directly excited Mn^{2+} ions. To investigate this effect the change in the ratio of the initial intensity of the longer lifetime to the total intensity as a function of pulse width (accomplished by masking the chopper aperture) was measured at 295 K and plotted in Fig. 7. The data indicate that the ratio remains essentially constant below pulse widths of 5 ms and then increases, becoming constant again for pulse widths greater than ~200 ms.

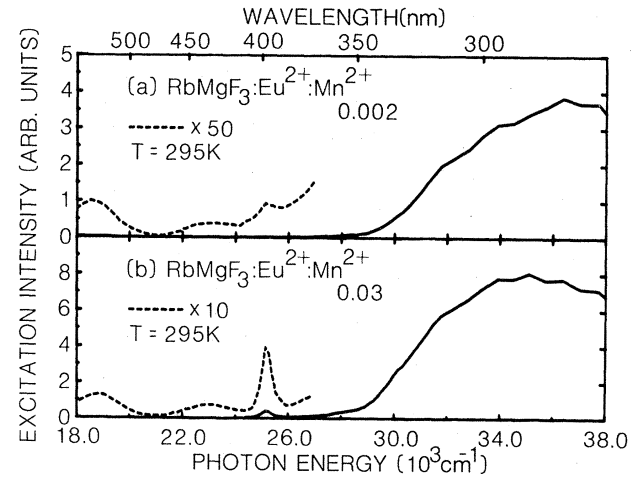

FIG. 5. (a) Excitation spectrum of Mn^{2+} in $RbMgF_3:Eu^{2+}:Mn_{0.002}{}^{2+}$ at 295 K. Bands plotted as dotted lines have had their intensities increased a factor of 50. (b) Excitation spectrum of Mn^{2+} in $RbMgF_3:Eu^{2+}:Mn_{0.03}{}^{2+}$ at 295 K. Bands plotted as dotted lines have had their intensities increased a factor of 10. In both figures the resolution was 5 nm and $\lambda_{em}=600$ nm.

IV. DISCUSSION

A. Energy transfer

Many studies on sensitized luminescence have used Mn^{2+} ions as activators.[31,32] More recently, experiments have been conducted on Eu^{2+}-Mn^{2+} energy transfer.[33–37] The presence of the band due to Eu^{2+} ion absorption in the Mn^{2+} excitation spectra (Fig. 5) is confirmation of energy transfer from Eu^{2+} ions. Figure 8 illustrates the excellent overlap between the Eu^{2+} $^6P_{7/3}$ emissions and the Mn^{2+} $^4T_{2g}$ (Ref. 2) absorption in $RbMgF_3$. This evidence and the decrease in the Eu^{2+} lifetimes in the $Mn_{0.03}{}^{2+}$ sample (Fig. 4) are indicative that energy transfer occurs from the Eu^{2+} $^6P_{7/2}$ level to the Mn^{2+} ions.

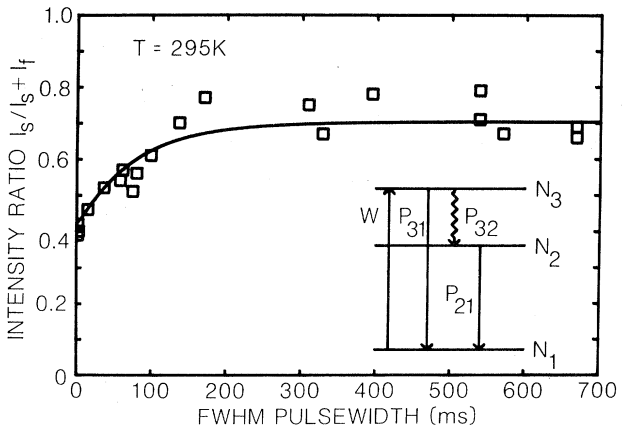

FIG. 7. Intensity ratio of the long lifetime decay to the total decay of the Mn^{2+} emission immediately after excitation ($\lambda_{ex}=318$ nm) vs the full width at half maximum pulsewidth of the excitation for $RbMgF_3:Eu^{2+}:Mn_{0.002}{}^{2+}$ at 295 K. The line is a least-squares fit to the data. Also shown is a diagram of the rate equation model upon which the fitting equation was based.

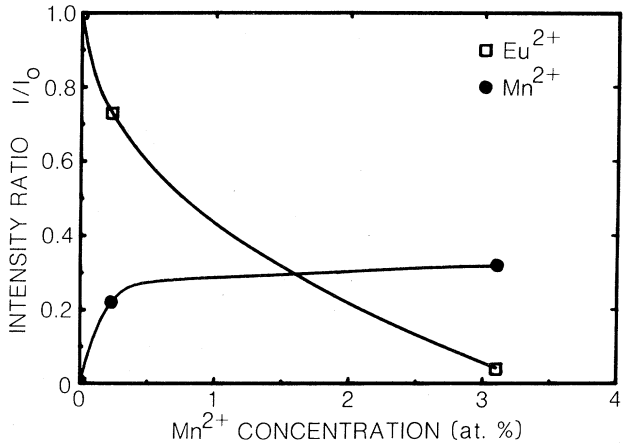

FIG. 9. Intensities of the Eu^{2+} and Mn^{2+} emissions as a function of Mn^{2+} concentration. The intensities are normalized to the intensity I_0 of $RbMgF_3:Eu^{2+}$.

Since sensitized luminescence occurs in $RbMgF_3$:Eu,Mn with the Eu^{2+} ions as sensitizers and the Mn^{2+} ions as activators, it is important to determine the type of energy transfer process (electric dipole-dipole, electric dipole-quadrupole, etc.). A prime assumption in energy transfer theories is the random arrangement of sensitizers and activators throughout the lattice.[1–6] Such a random arrangement constrains the pair concentration to be 100–1000 times less than the total impurity concentration. From Fig. 9 it is apparent that considerable sensitization of Mn^{2+} ions occurs even at concentrations of 0.2 at. %. If the arrangement of Eu^{2+} and Mn^{2+} ions is truly random then energy transfer would have to occur between ions separated, on the average, by over 20 Å. The energy transfer would have to be extremely efficient over this range, since the rise time of the Mn^{2+} luminescence in the $Mn_{0.002}{}^{2+}$ samples is faster than 50 ns.[38] If a *preferential pairing* or precipitation of the sensitizer and activator occurred, considerable sensitization would result, even at low concentrations of both types of ions. Such an aggregation could occur to reduce the strain in the lattice induced by the presence of the sensitizer or activator alone.[31] Previous studies on $RbMgF_3$:Mn (Refs. 12 and 25) and $RbMGF_3$:Er,Mn (Ref. 17) have shown that Mn^{2+} ions are randomly distributed in the lattice. The same techniques applied to the Mn^{2+}-doped samples used here also show that the Mn^{2+} ions are randomly distributed. This precludes the possibility of precipitates.

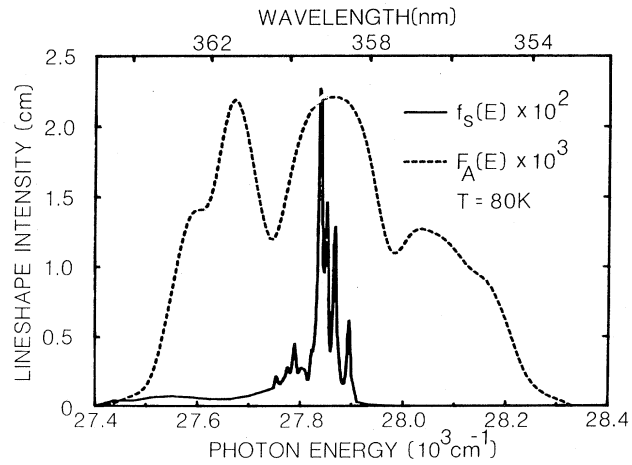

FIG. 8. Normalized line shapes of the Eu^{2+} $^6P_{7/2}$ emission (solid line) and Mn^{2+} $^4T_{2g}$ (Ref. 2) absorption (dotted line) at 80 K.

The following model would be consistent with the data: At the low concentrations of Eu^{2+} and Mn^{2+} in the $Mn_{0.002}{}^{2+}$ sample, pairing of the two ion types occurs at adjacent Rb^+ and Mg^{2+} sites. At this distance ($\sim$3.5 Å), energy transfer proceeds at a rapid rate which quenches the sensitizer luminescence completely. Unpaired sensitizers are, on the average, at a distance from the activator such that no energy transfer occurs, leaving the lifetime of the sensitizers unchanged. The data in Fig. 4 show that, within experimental error, the Eu^{2+} lifetimes of $RbMgF_3:Eu^{2+}$ and the $Mn_{0.002}{}^{2+}$ samples are the same. At higher activator concentrations the number of Eu^{2+}-Mn^{2+} pairs increase. Also, the distance between the unpaired sensitizers and activators is sufficiently reduced for energy transfer to occur. This is the case for the $Mn_{0.03}{}^{2+}$ samples which show fast energy transfer (the large initial fluorescence) as well as slower energy transfer (the fluorescence rise) from Eu^{2+} to Mn^{2+} ions after pulsed excitation.

To test this model we consider the simplified case where both the sensitizer and activator have only two levels, the ground and excited states. Actually, for both ion types the absorption is at a different level than emission, but nonradiative processes efficiently transfer all excitation to the lowest excited state. The intensity of the emission at frequency ν is related to the number of emitting ions in the following way:[39]

$$I(\nu)=N_e p^r h\nu\,, \tag{3}$$

where N_e is the number of emitting ions, p^r is the radia-

tive rate of the transition, and $h\nu$ is the energy of the emitted photon. If nonradiative processes can also depopulate the ion's emitting state, Eq. (3) must be modified using the expression

$$N_e = N\tau_f p^r , \tag{4}$$

where N is the number of excited ions, τ_f is the fluorescent lifetime;

$$\tau_f^{-1} = p^r + p^{nr} \tag{5}$$

and the nonradiative rate is p^{nr}. From Eq. (3)

$$I_{Mn} = N_{Eu\text{-}Mn} p^r_{Mn} h\nu_{Mn} , \tag{6}$$

$$I_{Eu} = N_{e\ Eu} p^r_{Eu} h\nu_{Eu} . \tag{7}$$

Since I_{Eu} arises from unpaired Eu^{2+} ions then N in Eq. (4) is replaced by

$$N = N_{Eu} - N_{Eu\text{-}Mn} . \tag{8}$$

At room temperature, $\tau_f p^r = 0.65$ where p^r is assumed equal to the inverse of the low-temperature lifetime (~ 2 ms). When the emission curves in Fig. 2(a) were integrated it was found that $I_{Mn} = 0.3 I_{Eu}$. With the use of this information and the above relations

$$N_{Eu\text{-}Mn} p^r_{Mn} h\nu_{Mn} = (0.3)(0.65)(N_{Eu} - N_{Eu\text{-}Mn}) p^r_{Eu} h\nu_{Eu} . \tag{9}$$

The peak intensity energies, $h\nu_{Mn}$ and $h\nu_{Eu}$, are at about 16 670 and 27 780 cm^{-1}, respectively. As mentioned earlier, the Mn^{2+} luminescence decay for the $Mn_{0.002}{}^{2+}$ samples is composed of two exponentials. The double-exponential decay is probably due to luminescence from two classes of Mn^{2+} ions. If we assume the faster temperature-independent lifetime class of ions to be more numerous, then the radiative rate p^r_{Mn} is essentially the inverse of the lifetime. Substituting the above values of p^r_{Mn}, p^r_{Eu}, $h\nu_{Mn}$, and $h\nu_{Eu}$ into Eq. (9), and solving for the ratio $N_{Eu\text{-}Mn}/N_{Eu}$ it was found that

$$\frac{N_{Eu\text{-}Mn}}{N_{Eu}} \approx 0.8 . \tag{10}$$

This result suggests that 80% of the Eu^{2+} ions are paired with Mn^{2+} ions so the intensity of the Eu^{2+} emission in the $Mn_{0.002}{}^{2+}$ samples should be $\sim 20\%$ of what it is for a $RbMgF_3$:Eu crystal with no Mn^{2+}. If the longer lifetime class of ions is considered to be the dominant class of fluorescent ions then the number of paired ions would be an even greater percentage of the total number of Eu^{2+} ions. The data in Fig. 9 show the intensity of the Eu^{2+} emission in the $Mn_{0.002}{}^{2+}$ samples to be 70% of the intensity of $RbMg_3$:Eu. It is to be admitted that numerous uncertainties exist in measurements of different crystals, nevertheless, the data in Fig. 9 suggest a lower limit on the number of Eu^{2+}-Mn^{2+} pairs of 30%. Thus it is reasonable to state that 30—80 % of the Eu^{2+} ions in the $Mn_{0.002}{}^{2+}$ crystals are paired. Calculation of the number of Eu^{2+}-Mn^{2+} pairs for the $Mn_{0.03}{}^{2+}$ sample is complicated by the effect of energy transfer on the Eu^{2+} lifetimes. If the approximation is made that the radiative rates of the Eu^{2+} and Mn^{2+} ions do not change significantly then the ratio $N_{Eu\text{-}Mn}/N_{Eu} \approx 0.95$ is in good agreement with the data in Fig. 9.

Further support for Eu^{2+}-Mn^{2+} pairs in $RbMgF_3$ comes from the application of the Förster-Dexter model[1–4] to the experimental data. The expression for the electric dipole-dipole transfer probability P_{dd} is given by[4]

$$P_{dd} = \frac{3h^4c^4}{4\pi n^4 \tau_s} \left[\frac{1}{R_{sa}}\right]^6 Q_A \int \frac{f_s(E) F_A(E) dE}{E^4} , \tag{11}$$

where τ_s is the radiative lifetime of the sensitizer, and R_{sa} is the distance between the sensitizer and activator. Also $Q_A = \int \sigma_A(E) dE$, where $\sigma_A(E)$ is the absorption cross section found by dividing the absorption coefficient at energy E by the concentration of ions. The normalized line-shape functions for the sensitizer and activator are given by $f_s(E)$ and $F_A(E)$, respectively, so that

$$\int f_s(E) dE = 1 , \tag{12}$$

$$\int F_A(E) dE = \int \frac{\sigma_A(E)}{Q_A} dE = 1 . \tag{13}$$

The emission spectrum of $RbMgF_3$:Eu at 80 K, shown in Fig. 8, was used to calculate $f_s(E)$. The absorption spectrum of the $^4T_{2g}$ (Ref. 2) level in a $Mn_{0.03}{}^{2+}$ sample was used for $F_A(E)$. This should introduce no error since Q_A will be concentration independent at the low activator concentrations used. Since the value of E in the denominator of the integral is almost constant over the range of integration it is usually given the value at the center of the overlap region and taken outside the integral. When these values were determined, it was found that $Q_A = 1.05 \times 10^{-19}$ $(cm^{-1})^{-1}$ and $\int f_s(E) F_A(E) dE = 1.87 \times 10^{-3}$ $(cm^{-1})^{-1}$. For $RbMgF_3$, $n = 1.48$ and $E = 27\,855.2$ cm^{-1}. Thus Eq. (11) can be written as

$$P_{dd} = \frac{1}{\tau_s} \left[\frac{4.7\ \text{Å}}{R_{sa}}\right]^6 \tag{14}$$

when R_{sa} is expressed in Å. The critical interaction distance R_0 is defined as that distance at which $P_{dd}\tau_s = 1$.[9] From Eq. (14) $R_0 = 4.7$ Å. For distances greater than R_0, the effect of electric dipole-dipole energy transfer is small. The simplest case for estimating the energy transfer rate between sensitizers and activators is when two energy levels are taken to characterize these ions. If the energy transfer rate P_{sa} is time independent then the number of excited activators following pulsed excitation is given by[9]

$$N_a(t) = P_{sa} N_s(0) / (p^r_A - p^r_s - P_{sa}) \{\exp[-(p^r_s + P_{sa})t] - \exp(-p^r_A t)\} , \tag{15}$$

where $N_s(0)$ is the initial population of the sensitizer's excited state immediately after the pulse, and p^r_s and p^r_A are the radiative rates of the sensitizer and activator, respectively. The time t_{max} at which the activator intensity is a maximum may be found by taking the time derivative of Eq. (15) and setting it to zero:

$$t_{\max}=\frac{1}{p_A^r-p_s^r-P_{sa}}\ln\left[\frac{p_A^r}{p_s^r+p_A^r}\right]. \quad (16)$$

It was stated earlier that for the $Mn_{0.002}{}^{2+}$ sample $t_{\max}<50$ ns. Since the data indicate that $p_s^r=500\ s^{-1}$ and $p_A^r=40\ s^{-1}$ then P_{sa} must be $\gtrsim 3\times10^8\ s^{-1}$. Inspection of Eq. (14) indicates that this fast energy transfer rate cannot be achieved through an electric dipole-dipole interaction.

The long lifetime of the Mn^{2+} ions is indicative of the forbiddenness of the transition. It is reasonable to assume that the energy transfer process may proceed via an electric dipole-quadrupole interaction.[4,36] The transfer rate for the electric dipole-quadrupole interaction is related to the transfer rate for the electric dipole-dipole interaction through the relation[9]

$$P_{dq}=\left[\frac{\lambda}{R_{sa}}\right]^2\left[\frac{f_q}{f_d}\right]P_{dd}\ , \quad (17)$$

where λ is the wavelength of the transition, and f_q,f_d are the oscillator strengths of the quadrupole and dipole transitions, respectively. The dipole transition has an oscillator strength of about 10^{-7} and the quadrupole transition has an oscillator strength estimated at 10^{-10}.[36,39] Since the transition occurs at $\sim$360 nm, substitution of these values into Eq. (17) yields

$$P_{dq}=\frac{1\times10^{-3}}{\tau_s}\left[\frac{24.6\ \text{Å}}{R_{sa}}\right]^8. \quad (18)$$

For $\tau_s=2$ ms and $R_{sa}=3.5$ Å, $P_{dq}=3\times10^6\ s^{-1}$ which is much closer to the P_{sa} value predicted from the rise time experiments. Better agreement may be obtained assuming the interaction is electric quadrupole-quadrupole or exchange in nature.[4,9,36,39] When Eq. (16) is applied to the value of $t_{\max}=780\ \mu$s for the $Mn_{0.03}{}^{2+}$ samples a value of $\sim6080\ s^{-1}$ for P_{sa} was obtained. This value, substituted into Eq. (18) yields $R_{sa}=7.6$ Å, in good agreement with the predicted value of 7 Å for unpaired sensitizers and activators when a uniform distribution is assumed. Thus the calculations based on the Förster-Dexter model of energy transfer indicate the observed rise times of the Mn^{2+} samples can only be explained if a short-range interaction such as electric dipole-quadrupole or exchange is active. This is in agreement with the close pair model introduced earlier. It should be emphasized that the pairing appears to be preferential and not random. For a random distribution the statistical number of Eu^{2+}-Mn^{2+} pairs would be given by

$$N_{\text{Eu-Mn}}=\frac{6N_{\text{Eu}}N_{\text{Mn}}}{N_{\text{Mg}}}. \quad (19)$$

If the Eu^{2+}-Mn^{2+} pairs were present in a random distribution then for a constant Eu^{2+} concentration of 2000 ppm there would be 3×10^{17} pairs/cm^3 in the $Mn_{0.002}{}^{2+}$ sample and 4.5×10^{18} pairs/cm^3 in the $Mn_{0.03}{}^{2+}$ crystal. This would result in a 15-fold increase in Mn^{2+} emission which is not consistent with the data in Fig. 9.

It was mentioned earlier that the aggregation of impurity ions with the appropriate radii would reduce elastic distortion of the lattice. The Eu^{2+} ion (1.12 Å) is smaller than the Rb^+ ion (1.48 Å) it replaces, while the Mn^{2+} ion (0.80 Å) is larger than the Mg^{2+} ion (0.65 Å). Earlier investigations have suggested pairing between sensitizers and Mn^{2+} ions in other hosts.[35,36,40,41] Investigations on Eu^{2+}-doped alkali halides have shown that Eu^{2+} precipitates form at room temperature.[42] Other studies have reported precipitation of Pb^{2+}-Mn^{2+} and Cu^+-Mn^{2+} in alkali halides.[43,44] These investigations have also shown that the precipitates could be dissolved through thermal annealing. When samples of both types of Mn^{2+}-doped crystals were quenched from 800 K no changes in the absorption or emission spectra were noted. This is most likely because the hexagonal $RbMgF_3$ structure inhibits mobility of the Eu^{2+}-cation vacancy, which is necessary to form aggregates.

B. Optical properties

Although the Eu impurity was added in trivalent form, it is incorporated into the $RbMgF_3$ lattice as Eu^{2+}. The presence of Eu^{2+} band or line emission depends on parameters such as the type of anion, the charge of the neighboring cations, and the size of the cation the Eu^{2+} ion replaces.[45] The presence of Eu^{2+} line emission, shown in Fig. 2, is indicative of a relatively low crystal field at the Eu^{2+} ion site. This is consistent with the Eu^{2+} ion substituting in the relatively open Rb^+ ion sites of the lattice. As noted earlier the number of f-f emission lines observed are indicative that several sites exist for the Eu^{2+} ion in this lattice.[18] From the lifetime data in Table I and the spectra shown in Fig. 3 at least eight sites are present. Examination of the $RbMgF_3$ crystal structure[11] shows that two types of Rb^+ sites exist, one with C_{3v} symmetry, the other with D_{3h} symmetry. When vacancies necessary for charge compensation are considered, the local and nonlocal compensation will result in five types of sites. Since there are more sites present, other modifications to the local environment must occur. The increase in the 359.8-nm emission as the Mn^{2+} concentration increases (Fig. 3) suggests that impurities could be responsible for other Eu^{2+} sites. Recent time-resolved spectroscopy measurements indicate that energy transfer occurs between ions responsible for the 360.5- and 361.25-nm emissions.[46] These ions must be close to one another, causing the shift apparent in the excitation spectra for these ions' emissions.

Evaluations of $RbMgF_3$:Eu^{2+} (Ref. 18) and $KMgF_3$:Eu^{2+} (Ref. 47) crystals grown at this institution show band emissions unmentioned in previous investigations.[48–50] Our crystals were grown with $EuCl_3$ as the impurity, rather than EuF_3. Because of this difference in growing procedure, it was believed that the 405- and 525-nm bands may be due to Cl^- ions substituting for F^- ions near the Eu^{2+} site. A $RbMgF_3$ crystal doped with EuF_3 has since been grown. Room-temperature measurements indicate that in all respects it is identical to the earlier crystal. Calculation of the integrated intensities of the 405-nm band and 360-nm line emissions in a $Mn_{0.002}{}^{2+}$ specimen, and use of Eqs. (3) and (4) results in an estimated concentration of about 10^{16} cm^{-3} for the Eu^{2+} ions responsible for the 405-nm emission. The concentration of

the Eu^{2+} ions which emit at 525 nm is of the same order. Only the high oscillator strength (~ 0.01) allows such a low concentration of emitters to be visible. At concentrations this low, it is possible that the band emissions are due to Eu^{2+} ions at dislocations or near impurities.

The optical properties of the Mn^{2+} ions were quite different in many respects for the two types of Mn^{2+}-doped samples. In the $Mn_{0.002}{}^{2+}$ samples the decay was the sum of two exponentials. This behavior, and the behavior exhibited in Fig. 7, may be explained by assuming that two classes of Mn^{2+} ions are independently excited. The Mn^{2+} ion lower energy levels may be reduced to an equivalent three-level system, shown schematically in Fig. 7. The population of level 2 during square-wave excitation of duration τ is given by the expression[39]

$$N_2(t)=D+E\exp(s_1 t)+F\exp(s_2 t),\quad t\leq\tau\ , \tag{20}$$

where

$$D=\frac{WN_0p_{32}}{s_1s_2}\ , \tag{21}$$

$$E=\frac{WN_0p_{32}}{s_1(s_1-s_2)}\ , \tag{22}$$

$$F=\frac{WN_0p_{32}}{s_2(s_2-s_1)}\ , \tag{23}$$

and s_1, s_2 are given by

$$\left.\begin{matrix}s_1\\ s_2\end{matrix}\right\}=\tfrac{1}{2}\{-(p_3+2W+p_{21}) \pm[(p_3+2W-p_{21})^2-4Wp_{32}]^{1/2}\} \tag{24}$$

and $N_0=N_1+N_2+N_3$, p_{32} is the rate of the nonradiative transition between levels 3 and 2, p_{31} and p_{21} are the radiative rates of levels 3 and 2, respectively, and $p_3=p_{31}+p_{32}$. The pump rate W is defined as the absorption cross section times the incident flux. For excitation of the Eu^{2+} ions and subsequent energy transfer to Mn^{2+} ions, $W\approx 1\times 10^{-4}\ s^{-1}$. For the conditions present in the Mn^{2+} system, i.e., $N_0\approx 10^{19}\ cm^{-3}$, $p_{21}\approx p_{31}\ll p_{32}\approx 1\times 10^6$, Eqs. (20)–(24) simplify and Eq. (20) becomes

$$N_2(t)\approx\frac{WN_0}{p_{21}}[1-\exp(-p_{21}t)]+\frac{WN_0}{p_3}\exp(-p_3 t)\ , \quad t\leq\tau \tag{25}$$

for $t\geq 50\ \mu s$ the second term becomes negligibly small so

$$N_2(t)\approx\frac{WN_0}{p_{21}}[1-\exp(-p_{21}t)]\ . \tag{26}$$

The intensity of the two classes of Mn^{2+} ions immediately following excitation is given by substituting Eq. (26) in Eq. (3),

$$I(\tau)=\frac{WN_0}{p_{21}}[1-\exp(-p_{21}\tau)]p^r h\nu\ . \tag{27}$$

Here p_{21} is the measured decay rate of level 2, which may be equal to p^r. The data in Fig. 7 were fitted to the ratio I_s/I_s+I_f where I is given by Eq. (27) and the subscript s or f denotes the slow or fast lifetime class of ions, respectively. The data in Fig. 6 may be used to assign values to all parameters in Eq. (27) except the product WN_0, which is of the order $10^{15}\ s^{-1}cm^{-3}$. The line shown in Fig. 7 is the fit to the data with $h\nu_F=h\nu_s$, $p_{21f}=p_f^r=38.5\ s^{-1}$, $p_{21s}=11.5\ s^{-1}$, $p_s^r=8.25\ s^{-1}$, $W_sN_{0s}=1.3\times 10^{15}\ s^{-1}cm^{-3}$, and $W_fN_{0f}=3.8\times 10^{14}\ s^{-1}cm^{-3}$. The excellent fit to the data supports the proposed model. It is more difficult to explain why two classes of ions exist; but considering that there are two Mg^{2+} sites in $RbMgF_3$,[16] one site of nearly O_h symmetry, the other site being considerably more constricted, the oscillator strengths of the Mn^{2+} ions in these sites may change, or changes may occur through exchange interactions, as was reported for Cu^+ and Mn^{2+} ions in $KZnF_3$.[51]

Comparison of the absorption and emission data shown in Figs. 1–3 and the Mn^{2+} lifetime data in Fig. 6 indicates that changes occur in the Mn^{2+} ion's optical properties when the Mn^{2+} concentration increases. These differences in optical properties are most likely due to the large number of Mn^{2+} ions which are not paired to Eu^{2+} ions. Based on the arguments presented earlier, this number will exceed 80% of the total Mn^{2+} concentration for the $Mn_{0.03}{}^{2+}$ sample. These Mn^{2+} ions will cause changes in the lattice which in turn affect the emission curves and decay times.[13]

V. CONCLUSION

This study has shown that Eu^{2+} ions sensitize Mn^{2+} luminescence in $RbMgF_3$ crystals. The energy transfer is due to resonance between the Eu^{2+} $^6P_{7/2}$ f-f emission and the Mn^{2+} $^4T_{2g}$ (Ref. 2) absorption, with subsequent luminescence from the $^4T_{1g}$ level. Integrated intensity and lifetime measurements as well as energy transfer rates calculated using the Förster-Dexter model suggest that Eu^{2+} ions pair with Mn^{2+} ions. The number of pairs formed is much greater than that expected for a statistical distribution. This pairing most likely occurs to reduce the strain in the $RbMgF_3$ lattice which results from the introduction of either impurity alone, and occurs as the crystal is grown. As the Mn^{2+} concentration is increased energy transfer between unpaired Eu^{2+} and Mn^{2+} ions occurs as well. No evidence was found for aggregate formation after crystal growth. These observations indicate that impurity ions of the appropriate ionic radii "prefer" to be paired. This implies that emission systems can be made with selected impurity ions which immensely enhance the sensitized luminescence.

ACKNOWLEDGMENTS

We thank D. K. Sardar for performing some of the lifetime and quenching experiments, and R. C. Powell and G. E. Venikouas for helpful discussions and the fast lifetime data. This work was supported by National Science Foundation Grant No. DMR-81-05017.

[1]T. Förster, Ann. Phys. 2, 55 (1948).
[2]T. Förster, Z. Naturforsch. 4a, 321 (1949).
[3]T. Förster, Discuss. Faraday Soc. 27, 7 (1959).
[4]D. L. Dexter, J. Chem. Phys. 21, 836 (1953).
[5]M. Inokuti and F. Hirayama, J. Chem. Phys. 43, 1978 (1965).
[6]M. Yokota and O. Tanimoto, J. Phys. Soc. Jpn. 22, 779 (1967).
[7]R. G. Bennett, J. Chem. Phys. 41, 3037 (1964).
[8]L. A. Riseberg and M. J. Weber, in *Progress in Optics,* edited by E. Wolf (Elsevier, New York, 1976), Vol. 14, p. 89.
[9]R. C. Powell and G. Blasse, in *Structure and Bonding,* edited by J. D. Dunitz, J. B. Goodenough, P. Hemmerich, J. A. Ibers, C. K. Jørgensen, J. B. Neilands, D. Reinen, and R. J. P. Williams (Springer, Berlin, 1980), Vol. 42, p. 43.
[10]C. M. Lawson, E. E. Freed, and R. C. Powell, J. Chem. Phys. 76, 4171 (1982).
[11]N. Koumvakalis and W. A. Sibley, Phys. Rev. B 13, 4509 (1976).
[12]W. A Sibley and N. Koumvakalis, Phys. Rev. B 14, 35 (1976).
[13]N. Koumvakalis, W. A. Sibley, and G. E. Venikouas, J. Lumin. 15, 283 (1977).
[14]W. A. Sibley and N. Koumvakalis, J. Phys. C 10, 4909 (1977).
[15]A. Podinsh and W. A. Sibley, Phys. Rev. B 18, 5921 (1978).
[16]M. D. Shinn, J. C. Windscheif, D. K. Sardar, and W. A. Sibley, Phys. Rev. B 26, 2371 (1982).
[17]D. K. Sardar, M. D. Shinn, and W. A. Sibley, Phys. Rev. B 26, 2382 (1982).
[18]R. Alcala, D. K. Sardar, and W. A. Sibley, J. Lumin. 27, 273 (1982).
[19]D. K. Sardar, W. A. Sibley, and R. Alcala, J. Lumin. 27, 401 (1982).
[20]J. Hernandez, W. K. Cory, and J. Rubio, Jpn. J. Appl. Phys. 18, 533 (1979).
[21]M. J. Freiser, S. Methfessel, and F. Holtzberg, J. Appl. Phys. 39, 900 (1968).
[22]W. A. Sibley, S. I. Yun, and W. E. Vehse, J. Phys. C 6, 1105 (1973).
[23]N. S. Hush and R. J. M. Hobbs, in *Progress in Inorganic Chemistry,* edited by F. A. Cotton (Interscience, New York, 1968), Vol. 10, p. 259.
[24]W. A. Sibley and D. Pooley, in *Treatise on Material Science and Technology,* edited by H. Herman (Academic, New York, 1974), Vol. 5, p. 45.
[25]W. A. Sibley, Semicond. Insul. 5, 281 (1983).
[26]R. A. Hewes and M. V. Hoffman, J. Lumin. 3, 261 (1971).
[27]N. S. Al'tshuler, L. D. Livanov, and A. L. Stolov, Opt. Spektrok. 36, 127 (1974) [Opt. Spect. (USSR) 36, 72 (1974)].
[28]S. N. Bodrug, E. C. Valyashko, V. N. Mednikova, D. T. Sviridov, and R. K. Sviridov, Opt. Specktrok. 34, 312 (1973) [Opt. Spect. (USSR) 34, 176 (1973)].
[29]E. Munoz, J. L. Boldu', and G. Aquilar, J. Chem. Phys. 63, 4222 (1975).
[30]J. L. Prather, *Atomic Energy Levels in Crystals* (U.S. Department of Commerce, Washington, D.C., 1961), NBS Monograph 19.
[31]Th. P. J. Botden, Philips Res. Rep. 7, 197 (1952).
[32]C. C. Klick and J. H. Schulman, in *Solid State Physics,* edited by F. Seitz and D. Turnbull (Academic, New York, 1951), Vol. 5, p. 119.
[33]T. L. Barry, J. Electrochem. Soc. 115, 733 (1968).
[34]T. L. Barry, J. Electrochem. Soc. 117, 381 (1970).
[35]M. Tamatani, Jpn. J. Appl. Phys. 13, 950 (1974).
[36]A. L. N. Stevels and J. M. P. J. Verstegen, J. Lumin. 14, 207 (1976).
[37]J. L. Sommerdijk and A. L. N. Stevels, Philips Res. Rep. 37, 221 (1977).
[38]G. E. Venikouas (private communication).
[39]B. DiBartolo, *Optical Interactions in Solids* (Wiley, New York, 1968).
[40]R. Leach, J. Electrochem. Soc. 105, 27 (1958).
[41]B. L. Danielson, Phys. Rev. 142, 228 (1966).
[42]F. J. López, H. Murrieta, J. Hernández, and J. Rubio, Phys. Rev. B 22, 6428 (1980).
[43]C. Zaldo, F. J. López, and F. Jaque (private communication).
[44]F. Jaque, C. Zaldo, F. Cussò, and F. Agullo-López, Solid State Commun. 43, 123 (1982).
[45]G. Blasse, Phys. Status Solidi B 55, K131 (1973).
[46]G. E. Venikouas, A. M. Ghazzawi, and R. C. Powell, Bull. Am. Phys. Soc. 28, 536 (1983).
[47]D. K. Sardar (private communication).
[48]N. S. Al'tshuler, E. Kh. Ivoilova, and A. L. Stolov, Fiz. Tverd. Tela (Leningrad) 15, 2407 (1973) [Sov. Phys.—Solid State 15, 1602 (1973)].
[49]J. L. Sommerdijk and A. Bril, J. Lumin. 11, 363 (1976).
[50]J. L. Sommerdijk, A. Bril, and F. M. J. H. Hoex-strik, J. Lumin. 15, 115 (1977).
[51]J. Ferguson, H. J. Guggenheim, and E. R. Kraus, J. Phys. C 4, 1866 (1971).